HHS Public Access

Author manuscript

Cell Rep. Author manuscript; available in PMC 2024 August 15.

Published in final edited form as:

Cell Rep. 2024 June 25; 43(6): 114337. doi:10.1016/j.celrep.2024.114337.

Endogenous p53 inhibitor TIRR dissociates systemic metabolic health from oncogenic activity

Eva Tsaousidou[1,2], **Jędrzej Chrzanowski**[3], **Pascal Drané**[2], **Grace Y. Lee**[1], **Nadine Bahour**[1], **Zeqiu Branden Wang**[1], **Shijun Deng**[1], **Zhe Cao**[1], **Kaimeng Huang**[2], **Yizhou He**[2], **Mateusz Kaminski**[4], **Dominika Michalek**[3,6], **Ekin Güney**[1,7], **Kalindi Parmar**[2], **Wojciech Fendler**[2,3], **Dipanjan Chowdhury**[2,5,*], **Gökhan S. Hotamışlıgil**[1,5,8,*]

[1]Sabri Ülker Center for Metabolic Research, Department of Molecular Metabolism, Harvard T.H. Chan School of Public Health, Boston, MA 02115, USA

[2]Department of Radiation Oncology, Dana-Farber Cancer Institute, Boston, MA 02115, USA

[3]Department of Biostatistics and Translational Medicine, Medical University of Lodz, 92-215 Lodz, Poland

[4]Department of General Surgery, Medical University of Lodz, 90-153 Lodz, Poland

[5]Broad Institute of Harvard and MIT, Cambridge, MA 02142, USA

[6]Present address: Center for Public Health Genomics, University of Virginia, Charlottesville, VA 22908, USA

[7]Present address: Department of Pathology, University of California, San Francisco, San Francisco, CA 94143, USA

[8]Lead contact

SUMMARY

It is unclear whether metabolic health corresponds to reduced oncogenesis or vice versa. We study Tudor-interacting repair regulator (TIRR), an inhibitor of p53 binding protein 1 (53BP1)-mediated p53 activation, and the physiological consequences of enhancing tumor suppressor activity. Deleting TIRR selectively activates p53, significantly protecting against cancer but leading to a systemic metabolic imbalance in mice. TIRR-deficient mice are overweight and insulin resistant, even under normal chow diet. Similarly, reduced TIRR expression in human adipose tissue correlates with higher BMI and insulin resistance. Despite the metabolic challenges, TIRR loss

*Correspondence: dipanjan_chowdhury@dfci.harvard.edu (D.C.), ghotamis@hsph.harvard.edu (G.S.H.).

AUTHOR CONTRIBUTIONS

Conceptualization, E.T., D.C., and G.S.H.; methodology, E.T., J.C., and W.F.; investigation, E.T., J.C., P.D., Y.H., D.M., M.K., E.G., G.Y.L., K.H., S.D., Z.B.W., Z.C., and W.F.; visualization, E.T., J.C., and W.F.; funding acquisition, E.T., W.F., D.C., and G.S.H.; project administration, K.P., W.F., D.C., and G.S.H.; supervision, D.C. and G.S.H.; writing – original draft, E.T.; writing – review & editing, E.T., J.C., P.D., Y.H., W.F., D.C., and G.S.H.

DECLARATION OF INTERESTS

The authors declare no competing interests.

SUPPLEMENTAL INFORMATION

Supplemental information can be found online at https://doi.org/10.1016/j.celrep.2024.114337.

improves p53 heterozygous ($p53^{HET}$) mouse survival and correlates with enhanced progression-free survival in patients with various $p53^{HET}$ carcinomas. Finally, TIRR's oncoprotective and metabolic effects are dependent on p53 and lost upon p53 deletion in TIRR-deficient mice, with glucose homeostasis and orexigenesis being primarily regulated by TIRR expression in the adipose tissue and the CNS, respectively, as evidenced by tissue-specific models. In summary, TIRR deletion provides a paradigm of metabolic deregulation accompanied by reduced oncogenesis.

In brief

Tsaousidou et al. describe opposing roles for TIRR, an inhibitor of the tumor suppressor p53. TIRR loss in mice results in increased body weight and insulin resistance but protects from cancer. Similarly, low TIRR levels correlate with increased body mass index in patients with type 2 diabetes but increased survival in patients with various carcinomas.

Graphical Abstract

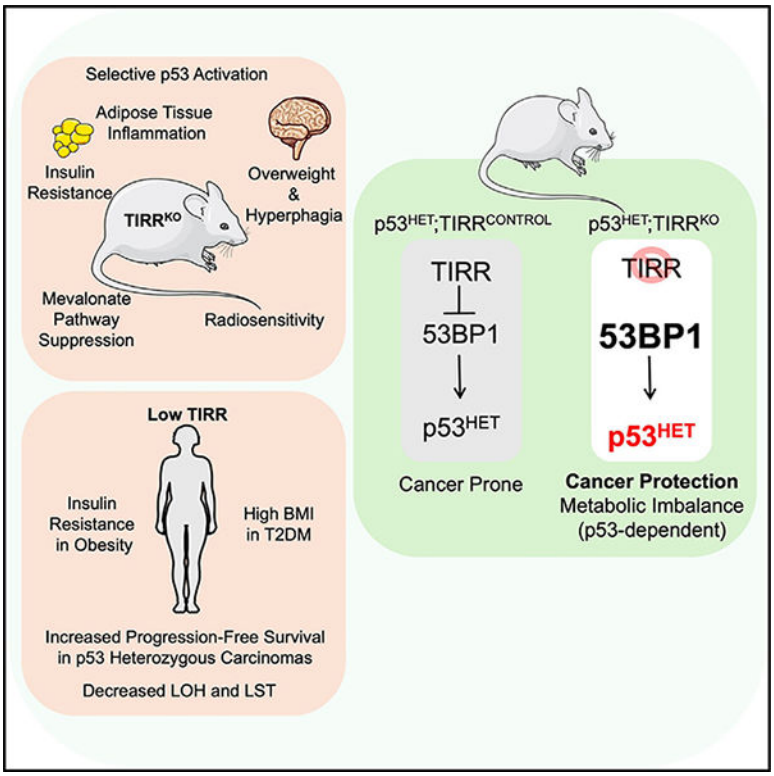

INTRODUCTION

The relationship between metabolism and cancer has gained scientific interest, in the context of both obesity and aging, two of the greatest risk factors in cancer development.[1,2] While tremendous progress has been achieved in understanding the cellular metabolism of cancer cells,[3] the microenvironment in oncogenic processes,[4] and the activity of many oncogenes and tumor suppressors,[5] as well as tumor-promoting cellular processes, such as impaired

DNA repair[6] and organelle dysfunction,[7] there remain uncertainties regarding the role of systemic metabolic health in cancer initiation and progression, especially in the context of obesity. Although the risk for metabolic pathologies and certain types of cancer is increased in obesity, it is unknown whether systemic metabolic health translates into oncoprotection or vice versa.

To approach this question, we utilized a newly identified endogenous inhibitor of p53. While upregulation of the activity of p53, a critical tumor suppressor, has been seen as a promising approach to combat tumor formation,[8] it has also been challenging, as excessive p53 activation leads to immoderate apoptosis, premature aging,[9] and even organismal death.[10–12] Interestingly, p53 activation is also described in obesity and linked to the emergence of metaflammation and insulin resistance.[13] As such, we envisioned that an endogenous, less potent, and tolerable model of selective p53 activation may be of great utility to address the relationship between systemic metabolism and oncogenic capacity, and we focused on the Tudor-interacting repair regulator (TIRR; alias Nudt16L1 and Syndesmos), a newly described p53 inhibitor. TIRR has been identified as an interaction partner of p53 binding protein 1 (53BP1) that keeps it off chromatin in the absence of DNA damage, thereby inhibiting its action.[14,15] 53BP1 is a multifaceted DNA repair protein that impacts genomic stability and enhances p53 function.[16,17] TIRR overexpression phenocopies 53BP1 ablation,[14] and in TIRR-depleted tumor cell lines, exogenous activators of p53 further enhanced p53-mediated gene transactivation, primarily via 53BP1.[18] Therefore, TIRR has been defined at the molecular level as a novel p53 inhibitor, but its significance and the potential applications of its suppression at the organismal level remain incompletely understood.

To enable the studies of TIRR *in vivo*, we developed mouse models to interrogate the role of TIRR in cancer, and the current study was inspired by the observation of significantly increased body weight in TIRR-deficient mice even when kept under standard laboratory conditions. Here, we show that TIRR suppression causes selective activation of endogenous p53, resulting in remarkable cancer prevention, only at the cost of systemic metabolic deregulation. TIRR's actions are p53 dependent, and in both normal physiology and cancer, its expression strongly correlates with p53-dependent cancer-preventive metabolic profiles, including the suppression of the cholesterol biosynthesis/mevalonate pathway. The absence of TIRR results in low-grade metabolic inflammation causing metabolic deregulation, with this phenotype also dependent on p53 and lost in a p53-deficient background.

RESULTS

TIRR ablation impairs the p53 response *in vivo*

To investigate the physiological role of TIRR, a novel p53 inhibitor (Figure 1A), at the organismal level, we generated mice with whole-body TIRR ablation by conditional mutagenesis. We targeted the first two, out of three total, exons of the TIRR gene, flanking them by *loxP* sites (Figure S1A). We validated the deletion of the first two exons of the TIRR gene by RNA sequencing (RNA-seq) analysis (Figure 1B) and real-time qPCR (Figure S1B). Mice with whole-body TIRR ablation were viable and fertile and did not present with gross developmental abnormalities. Bone mineral density as measured by dual-energy

X-ray absorptiometry (DEXA)-scan analysis (Figure S1C) and body length (Figure S1D) as well as blood cell counts (Figures S1E–S1G) were similar between the two experimental groups. Importantly, TIRR-knockout ($TIRR^{KO}$) mice also had a similar lifespan to their control littermates (Figure 1C), which is in stark contrast to mouse models with loss of Mdm2/Mdm4 (established inhibitors of p53) that result in embryonic lethality, which is only rescued by p53 ablation,[10–12] thereby limiting the opportunity to investigate the ectopic activation of endogenous p53 as a cancer-protective approach. Considering the TIRR/53BP1 relationship and 53BP1's profound impact on B cell maturation ($53BP1^{-/-}$ mice lose class switch recombination [CSR] capacity),[19] we examined CSR in TIRR-deficient animals. Confirming our previous findings that $53BP1^{-/-}$ primary B cells transduced with a 53BP1 mutant unable to bind TIRR had normal CSR capacity,[15] whole-body (Figure S1H) or B cell-specific TIRR ablation (Figures S1I and S1J) had no impact on CSR.

We next examined whether TIRR ablation affects the p53 response to stress. We studied the physiology of $TIRR^{KO}$ mice in the context of ionizing radiation (IR)-induced acute radiation syndrome, which is largely dependent on p53 activity. After testing for an optimal irradiation dose (Figure S1K), mice with whole-body TIRR ablation were significantly more sensitive (Figure 1D) ($p = 0.01$, log-rank/Mantel-Cox test) to total body irradiation (8.5 Gy) compared to their wild-type (WT) littermates. The final survival rate was 9.3% for the $TIRR^{KO}$ mice and 40% for the $TIRR^{WT}$ mice ($p = 0.03$, log-rank test). We hypothesized that this is due to increased p53 function and therefore measured the expression of p53-target genes in spleens of mice irradiated with a low dose of IR (2 Gy). Consistently, we observed an increase in the expression of multiple p53-target genes in $TIRR^{KO}$ mice compared to their WT littermates in spleen (Figure 1E) but not all of them (Figure S1L) and not in every tissue we examined (Figure S1M). Taken together, these results demonstrate that TIRR ablation does not impact the development or lifespan but increases the sensitivity of p53 to stress *in vivo*.

TIRR is important for maintaining metabolic balance

Interestingly, during the establishment of the colonies, we observed that $TIRR^{KO}$ mice were significantly heavier than their control littermates ($TIRR^{WT}$) even when fed a normal chow diet (NCD; Figure 1F). This observation stimulated further studies, as metabolic stress has also been implicated as an activator of p53 and shown to impair insulin sensitivity.[13,20] $TIRR^{KO}$ mice also developed other aspects of metabolic imbalance, such as glucose intolerance (Figure 1G) and insulin resistance (Figure S2A), hyperinsulinemia (Figure S2B), hyperglycemia (Figure S2C), hypercholesterolemia (Figure S2C; 25% increase, $p = 0.03$), hyperphagia (Figure S2D, 14% increase, $p = 0.02$), and increased whole-body adiposity (Figure S2E, 24% increase, $p = 0.02$), as also reflected by the increased perigonadal adipose tissue (PGAT) size compared to $TIRR^{WT}$ littermate mice (Figure S2F). $TIRR^{KO}$ mice also had enlarged average adipocyte size (Figure S2G) and significantly different adipocyte size distribution (Figure S2H) but unaffected non-esterified fatty acid (NEFA) and lean mass levels (Figures S2I and S2J) and circulating levels of adiponectin and leptin (Figures S2K and S2L). We also examined the average pancreatic islet surface area (Figure S2M) and respiratory exchange ratio (Figure S2N) and did not observe differences between genotypes. Notably, the differences in body weight and adiposity persist until the age of 30 weeks

(Figure S2O). Taken together, these results suggest a novel role for TIRR in systemic metabolic health, in the absence of additional dietary or genetic interactions.

As a first approach to validate TIRR's potential role in metabolic homeostasis in humans, we performed *in silico* analysis of publicly available data (GEO: GSE20950 and GSE15773)[21] and demonstrated that obese but insulin-sensitive humans have significantly increased omental adipose tissue TIRR expression compared to obese, insulin-resistant humans (Figure S3A). Moreover, in our cohort where we collected visceral fat from patients with type 2 diabetes that underwent bariatric surgery, we observed that TIRR expression inversely and significantly correlated with BMI (Figure 1H, $R = -0.73$, $p = 0.010$). These examples of high TIRR expression positively correlating with healthier metabolic status strengthened our observations from $TIRR^{KO}$ mice and supported the idea that TIRR may be an important regulator of metabolic balance and that this model would serve well to explore links, or lack thereof, between systemic metabolism and cancer. Our results so far have indicated that TIRR has a role in metabolic balance, but the physiological trigger for TIRR expression in the context of metabolism remained unclear. Metabolic stress has been indicated as a potential cause for p53 activation[20]; therefore, we postulated that TIRR might participate in the response to a high-fat diet (HFD), potentially through p53. Accordingly, we exposed WT mice to an HFD for 6 weeks and measured TIRR expression in PGAT, observing a significant increase of TIRR and p21, a major p53 target, expression compared to NCD (Figure S3B). To test TIRR's role in the conditions of metabolic challenge, we studied the *in vivo* physiology of $TIRR^{KO}$ mice under an HFD. In this setting, there were no statistically significant differences between control and $TIRR^{KO}$ littermate mice in body weight (Figure S3C), adiposity (Figure S3D), leptin (Figure S3E), and adiponectin levels (Figure S3F), as well as hypothalamic gene expression (Figure S3G). Interestingly, under an HFD, we still observed significantly impaired glucose homeostasis in whole-body $TIRR^{KO}$ mice (Figures S3H and S3I).

Transgenic overexpression of p53 in the adipose tissue has been demonstrated to disrupt glucose homeostasis.[13] Also, TIRR impedes the expression of canonical p53 target genes related to apoptosis and cell-cycle arrest in cancer cell lines and in breast and prostate carcinomas.[18] We asked whether there is a difference in expression of these classical p53 targets in tissues in normal physiology that may influence body weight. RNA-seq analysis revealed that in the absence of external stimulation, there is no difference in p53 target gene set expression between $TIRR^{WT}$ and $TIRR^{KO}$ littermate mice in liver, hypothalamus, PGAT, and brown adipose tissue (Figure S3J). However, this prompted us to focus on TIRR's specific role in the regulation of metabolic pathways. Therefore, we hypothesized that the effect of TIRR deficiency on metabolic balance might be due to the activation of a subset of p53 targets. To investigate transcriptional changes resulting from TIRR ablation, we conducted further analysis of the PGAT-derived RNA-seq data from $TIRR^{KO}$ mice and their WT littermates. In $TIRR^{KO}$ mice, gene set enrichment analysis (GSEA) revealed a significant upregulation of JAK/STAT signaling and cytokine-cytokine receptor signaling (Figure 1I) pathways, which are involved in low-grade metabolic inflammation, that can impact the dysregulation of glucose homeostasis.[22] Another major transcriptional program significantly downregulated in the PGAT of $TIRR^{KO}$ animals was the cholesterol biosynthesis pathway (Figures 1I and S3K from two independent mouse

cohorts), with its significant suppression further confirmed by real-time qPCR (Figure S3L). To validate this mechanistic insight of TIRR action in metabolic regulation, we used mouse embryonic fibroblasts (MEFs) derived from $TIRR^{KO}$ and $TIRR^{fl/fl}$ mice. Gene expression analysis by real-time qPCR (Figure S3M) revealed increased Abca1 expression in $TIRR^{KO}$ MEFs, which has been shown to be regulated by p53 to suppress the expression of mevalonate pathway—which includes the cholesterol biosynthesis pathway—genes in mice.[23] Increased Abca1 expression resulting in the suppression of mevalonate pathway genes (such as Hmgcs1 and Hmgcs2) was also observed in differentiated 3T3L1 adipocytes treated with small interfering RNA (siRNA) against TIRR (Figure 1J). Additionally, we evaluated the expression of other genes involved in metabolic regulation and inflammatory response in adipose tissue (Figure S4A), liver (Figure S4B), and quadriceps (Figure S4C) and could demonstrate that the main differences we observed were in the adipose tissue and particularly TIRR's role in suppression of the mevalonate pathway. Therefore, the suppression of cholesterol biosynthesis pathway expression, potentially due to selectively increased p53 activity, can serve as a consistent readout for gene expression regulation in the absence of TIRR, both in tissues (PGAT from independent mouse cohorts) and in cell culture (MEFs and differentiated 3T3L1), as the classical p53 target genes appear to be unaffected under physiological conditions.

Distinct tissue-specific roles for TIRR in the regulation of energy and glucose homeostasis

To address the relative contributions of different organs to the metabolic phenotypes of $TIRR^{KO}$ mice, we evaluated two additional *in vivo* mouse models. The observation of hyperphagia in $TIRR^{KO}$ mice prompted us to ablate TIRR in the CNS, the center of food intake regulation, by crossing the $TIRR^{fl/fl}$ mice with the Camk2a-Cre model. Genetic removal of TIRR in the CNS resulted in significantly increased body weight compared to control littermates, replicating the phenotype of $TIRR^{KO}$ mice under regular dietary conditions (Figure 2A). Strikingly, despite the presence of body weight deregulation, there were no alterations in glucose homeostasis in Camk2a-$Cre^{TG/WT}$;$TIRR^{fl/fl}$ mice (Figure 2B). The increased body weight of Camk2a-$Cre^{TG/WT}$;$TIRR^{fl/fl}$ mice was reflected in the increased PGAT weight (Figure 2C) and can be explained by the higher expression of orexigenic peptides, AgRP and NPY, in the hypothalamus compared to $TIRR^{fl/fl}$ mice (Figure S5A), which also translated into higher food intake (Figure S5B). Although we could not demonstrate the exact suppression of TIRR in hypothalamic neurons by Camk2a-Cre, due to the presence of multiple cell types that are not targeted by it, such as astrocytes and glial cells, we still observed significant Cre expression in the hypothalamus as demonstrated by qPCR (Figure S5C). Liver (Figure S5D) and adipose tissue (Figure S5E) gene expression was largely unaffected, strengthening our hypothesis that the metabolic phenotype we observed was due to TIRR's role in the hypothalamic regulation of food intake. Mechanistically, we postulate that the effect of TIRR on food intake might be via an increase in inflammatory pathway gene expression, such as tumor necrosis factor alpha (TNF-α) (Figure S5A), as hypothalamic inflammation has been demonstrated to dysregulate both energy and glucose homeostasis.[24]

In the absence of any abnormalities in glucose homeostasis in the CNS-specific TIRR ablation model, we explored whether the origin of this phenotype relates to TIRR's function

in the peripheral organs. As we have observed that adipose TIRR expression is altered during metabolic stress, adipose gene expression is significantly regulated in $TIRR^{KO}$ mice, and as the adipose tissue is crucial for glucose homeostasis, we generated adipose-tissue-specific TIRR-ablated mice by crossing the $TIRR^{fl/fl}$ mice to the AdipoQ-Cre model, achieving an over 80% suppression of TIRR gene expression in adipocytes in both exons 1 and 3 as measured by qPCR (Figure S5F). Interestingly, AdipoQ-$Cre^{TG/WT}$;$TIRR^{fl/fl}$ mice had a similar body weight (Figure 2D) and respiratory exchange ratio (Figure S5G) to their control littermates but were glucose intolerant (Figure 2E). Taking these results together, we could demonstrate that hypothalamic-specific TIRR ablation resulted in increased body weight, whereas adipose-specific TIRR ablation was sufficient to cause glucose homeostasis deregulation, both under NCD conditions, thus dissociating the two major causes for metabolic dysfunction in the whole-body $TIRR^{KO}$ mice (Figure 2F). We then investigated whether the transcriptional regulation observed in the adipose tissue after whole-body TIRR ablation is present in the adipose-specific model and demonstrated a significant overlap. Major metaflammatory mediators such as JAK/STAT (Figure S6A) and cytokine-cytokine receptor signaling pathways (Figure S6B), which were significantly upregulated in the whole-body TIRR ablation model, continued to be upregulated in the adipose-specific model. Importantly, the overlap between whole-body and adipose-specific models was also present in the terpenoid biosynthesis process, which is part of the mevalonate pathway (Figure S6C). These results demonstrate the distinct contributions of TIRR action in specific tissues.

TIRR's metabolic role is p53 dependent

Transcriptional profiles generated from cells and tissues with TIRR ablation collectively point to p53 regulation as a critical mechanism underlying the observed phenotypes. In an attempt to gain definitive mechanistic proof that p53 has a causative role for the metabolic deregulation in the absence of TIRR *in vivo*, we generated and examined p53 heterozygous ($p53^{HET}$);$TIRR^{KO}$ and $p53^{KO}$;$TIRR^{KO}$ mice against their respective control littermates. The metabolic imbalance of $TIRR^{KO}$ mice was present but milder in the presence of a single copy of p53. The $p53^{HET}$; $TIRR^{KO}$ mice were still significantly heavier under NCD conditions (Figure 2G) and exhibited glucose intolerance compared to control littermate mice, $p53^{HET}$;$TIRR^{CONTROL}$ (Figure 2H), as well as higher total adiposity (Figure 2I). The metabolic deregulation was completely normalized in the $p53^{KO}$ background; that is, the increased adiposity and hyperinsulinemia of $p53^{HET}$;$TIRR^{KO}$ mice were normalized in the $p53^{KO}$;$TIRR^{KO}$ model (Figures 2I and S6D–S6F). Additionally, $p53^{KO}$;$TIRR^{KO}$ mice had a similar body weight and glucose homeostasis to $p53^{KO}$;$TIRR^{CONTROL}$ animals (Figures 2J and 2K), providing clear evidence that TIRR's effect on metabolic health is p53 dependent *in vivo*. We also performed RNA-seq analysis to investigate the molecular alterations resulting from the phenotypic rescue of the TIRR ablation after the removal of p53. Principal-component analysis (PCA) of PGAT RNA-seq data revealed a clear distinction between the $p53^{WT}$;$TIRR^{KO}$ group and the $p53^{WT}$;$TIRR^{WT}$, $p53^{KO}$;$TIRR^{CONTROL}$, and $p53^{KO}$;$TIRR^{KO}$ groups (Figure S6G). Lastly, the significant suppression of the cholesterol biosynthesis pathway as seen by GSEA in $p53^{WT}$;$TIRR^{KO}$ mice compared to $p53^{WT}$;$TIRR^{CONTROL}$ mice in PGAT was completely reversed in the absence of p53 (Figure 2L). Other pathways affected by $TIRR^{KO}$ and reversed upon p53 ablation that

could contribute to the metabolic abnormalities of the TIRR^{KO} mice include increased JAK/STAT pathway and apoptosis and decreased oxidative phosphorylation, glycolysis, and peroxisomal gene expression. Taken together, our observations indicate that the metabolic imbalance in TIRR^{KO} animals is largely mediated by the selective ectopic transactivation function of p53 and may not involve classical p53 target genes involved in cell cycle.

Low TIRR expression correlates with increased cancer survival in a p53-dependent manner

The key question was whether the TIRR-mediated selective regulation of p53 impacts tumorigenesis in the face of disrupted systemic metabolism. Therefore, we studied the effect of TIRR deficiency in a model of spontaneous tumor development, the p53^{HET} cancer model. Mice with p53 heterozygosity develop tumors, primarily lymphomas and sarcomas.[25] Therefore, we generated p53^{HET};TIRR^{KO} mice and compared their survival to p53^{HET};TIRR^{CONTROL} littermate mice. The p53^{HET};TIRR^{KO} mice show dramatic protection from cancer with a significantly increased lifespan compared to p53^{HET};TIRR^{CONTROL} littermate mice (Figure 3A). We further determined that the lifespans of p53^{KO};TIRR^{KO} and p53^{KO};TIRR^{CONTROL} littermate mice were similar, serving as additional evidence that p53 proficiency is necessary for TIRR loss to induce tumor suppression (Figure 3B). The fact that there is no difference in the survival of p53^{KO}; TIRR^{KO} and p53^{KO};TIRR^{CONTROL} mice might suggest that the tumor-suppressive activity occurs at the level of tumor initiation rather than tumor progression, perhaps alleviating the selective pressure for p53 loss of heterozygosity (LOH) to initiate cell transformation. Accordingly, we hypothesized that low TIRR expression leading to enhanced 53BP1, and thereby p53, activity might impact genomic stability in primary tumors. Therefore, we assessed LOH, which is intrinsically linked to aggressive malignancies. We performed *in silico* analysis of The Cancer Genome Atlas (TCGA) and correlated TIRR expression with LOH and large-scale transitions (LSTs) as markers of genomic stability. Indeed, low TIRR expression significantly correlated with decreased LOH and LST in patients with stomach adenocarcinoma (Figures S7A and S7B), prostate adenocarcinoma (Figure S7C), and lung adenocarcinoma (LUAD; Figure S7D). In p53-proficient ovarian cancers, low TIRR expression correlated with decreased LSTs (Figure S7E), whereas 53BP1 expression presented with an inverse correlation (Figure S7F), providing an indication that the inhibitory regulation of TIRR on 53BP1 can be the mechanistic explanation of altered genomic stability. We further performed analysis on pancancer data and confirmed this observation for both LOH and LSTs. Importantly, TIRR's effect on LOH and LSTs is dependent on a functional nonhomologous end joining/homologous recombination pathway (Figures S7G and S7H, respectively).

Next, we examined whether low TIRR expression also translates into a better outcome/ survival in patients with cancer. We analyzed data from the Genomic Data Commons[26] of patients with primary LUAD (TCGA-LUAD) harboring one p53 allele loss (p53^{HET}). p53^{HET} was defined as one WT and one lost p53 allele. Due to the small number of double allele loss in cancer samples, we defined p53^{KO} as the loss of both p53 alleles (deep homodeletion) or the loss of a single allele with a concurrent loss-of-function dominant-negative coding-region variant. The reason we first focused on TCGA-LUAD was because

the number of samples with available clinical and sequencing data was statistically relevant, the highest compared to any other cancer type and with adequate representation of both sexes (53.64% females). From a total of 522 TCGA-LUAD cases, 507 had summarized genomic data available, out of which 317 had reported the first outcome treatment as a complete/partial response. After review of the mutational and copy-number status, 60 samples were defined as $p53^{HET}$ and 90 as $p53^{KO}$. We observed a significant increase in the progression-free survival (PFS) of $p53^{HET}$ patients with low TIRR expression ($n = 30$) relative to those with high TIRR ($n = 30$), as defined by the median (Figure 3C and Oncogrid in Figure S8A). The impact of low TIRR expression on PFS was absent in p53-deficient patients ($p53^{KO}$, Figure 3D). As TIRR is an endogenous inhibitor of 53BP1-mediated p53 activation, we next examined the potential correlation of 53BP1 expression to PFS of the same patient cohorts. In accordance with our working model, high 53BP1 expression (above the median) was associated with increased PFS ($p = 0.08$) compared to low 53BP1 expression in $p53^{HET}$ TCGA-LUAD patients (Figure S8B), an association that was completely lost in $p53^{KO}$ patients (Figure S8C). However, due to the small sample size, we were limited by statistical power to detect a true hazard ratio (HR) of 0.614 or 1.698. Hence, we decided to expand on the analysis using stratified Cox regression approach on pancancer data. Initial data included 32 different cancer cohorts and 1,923 samples, with only 15 cohorts that satisfied our selection criteria (at least 10 samples and at least 3 complete events). We performed a stratified analysis of the aforementioned 15 cohorts of primary $p53^{HET}$ cancers from public databases (including bladder urothelial, cervical squamous cell carcinoma, endocervical adenocarcinoma, colon adenocarcinoma, rectum adenocarcinoma, esophageal carcinoma, head and neck squamous cell carcinoma, LUAD, lung squamous cell carcinoma, ovarian serous carcinoma, pancreatic adenocarcinoma, pheochromocytoma and paraganglioma, prostate adenocarcinoma, stomach adenocarcinoma, uterine corpus endometrial carcinoma, and uterine carcinosarcoma) where the sample numbers (181 and 480 for $p53^{HET}$ and $p53^{KO}$, respectively) allowed for statistical reasoning with sufficient power. We observed that an increase of TIRR expression translated into an elevated risk for cancer progression by 45% ($n = 181$, HR = 1.4522 [95% confidence interval (CI): 1.0401–2.0274] per 1 SD, $p = 0.0285$, Figure 3E). Importantly, this increase in progression was p53 dependent, as it was not observed in $p53^{KO}$ cancers ($n = 480$, HR = 1.0076 [95% CI: 0.8759–1.1591] per 1 SD, $p = 0.9155$, Figure 3F). These results identify TIRR as a key player in the regulation of p53mediated tumor suppression (Figure 3F) and support the idea that TIRR inhibition may be an effective strategy to suppress the growth of p53-proficient cancers.

Low-TIRR/p53-dependent cancer benefits require the suppression of the mevalonate pathway

To establish a causative role between the transcriptomic changes due to TIRR suppression and the increased PFS in patients with $p53^{HET}$ LUAD and $p53^{HET}$ mice (Figures 3A and 3C), we utilized the observations of the transcriptomic profile of the $TIRR^{KO}$ models and compared it to that of the patients. Indeed, low TIRR expression still correlated with suppression of the cholesterol biosynthesis/mevalonate pathway (Figure 4A), as it did in the experimental $TIRR^{KO}$ model. Repression of the cholesterol/mevalonate pathway has already been shown to contribute to tumor suppression in a p53-dependent manner.[23,27]

Importantly, cholesterol biosynthesis suppression due to low TIRR was lost in the absence of p53 in TCGA-LUAD patients (Figure 4B). Mechanistically, increased p53 activity has been demonstrated to increase the expression of Abca1[23] and suppress Sqle,[27] which were both confirmed in TIRR^{KO} MEFs by chromatin immunoprecipitation (ChIP)-PCR (Figure 4C). Interestingly, we could observe an increase in ABCA1 protein levels in insulin-stimulated livers of TIRR^{KO} mice, again confirming previous observations of increased p53 activity (Figure S8D). Additionally, increased p53 activity has been shown to increase TNF-α expression,[13] which was also confirmed in TIRR^{KO} MEFs (Figure 4D), a regulation that was ABCA1 and therefore mevalonate pathway dependent. To further support the mechanistic link between 53BP1 and TIRR in this context, 53BP1 and TIRR suppression by siRNA in differentiated 3T3L1 adipocytes resulted in the normalization of ABCA1 mRNA expression levels, which were increased after TIRR alone (Figure S8E). Importantly, we could not observe any differences in total, acetylated, or phosphorylated levels of p53 after irradiation (Figure S8F). Furthermore, below-median TIRR expression in patients with p53^{HET} LUAD also correlated with increased p53 activation (Figure S8G). These indications serve as distinct signaling cascades that may cumulatively result in the increased survival of the patients.

Identification of a p53-dependent TIRR-specific transcriptomic signature

The investigation of tissue-specific models of TIRR ablation reinforced the validation of TIRR's physiological and pathological roles and allowed for further examination for the identification of a TIRR-specific transcriptomic regulation. To investigate this further, we generated a p53-dependent TIRR signature derived from MEFs of the TIRR^{KO} models and used it to define the specific gene expression changes that could be responsible for the extended PFS of patients with p53^{HET} LUAD with low TIRR expression and with the potential to be used as a prognostic tool (Figure 4E). Importantly, the p53-dependent TIRR signature correlated significantly with TIRR expression levels in patients with p53^{HET} LUAD (Figure 4F). The correlation was lost when the tumors were p53^{KO}, confirming the validity of the signature's composition (Figure S8H).

DISCUSSION

The impact of systemic metabolic disturbances on tumorigenesis and the underlying mechanisms remains incompletely resolved. Generally, it is believed that poor systemic metabolic control contributes to cancer development, with overlapping pathways often driving both metabolic disturbances and oncogenesis. However, our findings challenge this prevailing model. Removing TIRR led to increased body weight and insulin resistance but provided robust protection against cancer development by activating p53 activity. This represents an endogenous mechanism that sacrifices metabolic health for oncoprotection. This perspective may align with evolutionary considerations, where safeguarding genomic integrity and preventing oncogenesis hold greater importance than maintaining metabolic health, particularly in scenarios where the level of metabolic disruption does not pose an immediate threat to reproductive capacity or immediate survival.

TIRR has been biochemically characterized as a p53 inhibitor in mammalian tumor cell lines.[15,28,29] However, its physiological role at the organismal level was not known. In this study, using multiple mouse models, we elucidated the role of TIRR in physiology, which enabled us to further decipher its mechanistic role in cancer and its impact on systemic metabolism, both of which are dependent on the presence of intact p53, also using human patient data *in vivo*. TIRR^{KO} mice were viable, fertile, and had normal blood counts and an unaffected lifespan, in stark contrast to other p53 inhibitors whose ablation results in embryonic lethality[10–12] but comparing favorably with models of increased p53 activity in mice that had no effects on aging.[8] Notably, our study is also in accordance with previously published work on other p53 pathway players, such as studies demonstrating that increased Arf/p53 levels result in cancer resistance and have decreased levels of ageing-associated damage.[30] Loss of Mdm2/Mdm4 (established inhibitors of p53) results in embryonic lethality, which is only rescued by p53 ablation,[10–12] thereby limiting the opportunity to investigate the ectopic activation of endogenous p53 as a cancer-protective approach. This is also evident in the toxicity induced by Mdm2/4 inhibitors in both animal cancer models and human patients with cancer,[31] resulting in thrombocytopenia, leukopenia, and anemia.[32] Nevertheless, studies with Mdm2/4 heterozygous mice have indicated their importance as cancer drug targets.[33,34] From the cancer perspective, TIRR ablation in mice markedly reduced oncogenesis and increased survival in a p53^{HET} model. Consistent with this observation, patients with p53 heterozygosity and low TIRR expression had significantly increased PFS compared to patients with high TIRR expression in multiple cancer types.

We surmise that TIRR suppression resulted only in selective and tolerable activation of p53, which specifically suppresses the growth of dividing cancer cells but is not toxic for the whole organism. As such, our observations may provide a promising approach to leverage TIRR targeting in p53-proficient tumors. However, a fascinating conundrum would be the potential negative impact of TIRR inhibition on metabolic health and whether these observations will apply to humans or be tolerable in a short-term context.

TIRR deficiency resulted in the pronounced suppression of mevalonate pathway genes and increased metaflammatory signaling. Importantly, we observed the selectivity of TIRR's impact on p53-mediated gene expression. A comprehensive analysis of 44 datasets from human p53 ChIP-seq studies revealed that only 11% of all p53-bound sites near the transcription start site of genes result in differential expression.[35] The lack of correspondence between binding and expression suggests that additional context-dependent signals, such as cofactors, may be required for an efficient p53 transcriptional response. Our results indicated that only a subset of p53's extensive transcriptional network was regulated by TIRR/53BP1 in the context of metabolic stress, and Abca1 and Sqle are differentially regulated by p53 (Figure 4C), according to previously published studies.[23,27] Nevertheless, further studies are warranted to explore such pathways to further delineate the target preferences of p53 in metabolic vs. oncogenic contexts.

TIRR^{KO} mice presented with being overweight, glucose intolerance, and increased adiposity even under a normal diet. Interestingly, some of the metabolic pathologies related to TIRR deficiency emanate from its actions in the adipose tissue, a site that is crucial in

metabolism and physiology but not commonly studied in the context of cancer. It has been reported that exposure to an HFD, for as short as 2 weeks, and genetically induced obesity both result in p53 activation in the adipose tissue, despite its specialized energy-handling capacity.[20] Furthermore, transgenic p53 expression in the adipose tissue has been linked to metabolic inflammation and insulin resistance, which can be reversed by blocking TNF-α.[13] Strikingly, however, TIRR deficiency and p53 activation in the adipose tissue do not contribute to the overweight phenotype observed in whole-body deletion of the TIRR gene. Instead, our work demonstrated that the increased adiposity driven by TIRR targeting is driven entirely through TIRR deficiency in the CNS. In addition to offering important insights into TIRR action on metabolism through different target tissues, these results allow the speculation that a potential therapeutic modality would not expose the adipose tissue would be free of such undesired metabolic side effects. As adipose tissue malignant tumors are extremely rare, this may not compromise the desired therapeutic potency through TIRR-mediated modulation of p53. Similar considerations could also be made for entities that may not penetrate the blood-brain barrier; however, this may not be needed, as a moderate increase in adiposity without any metabolic consequences may be a tolerable side effect in the context of cancer treatment.

There are p53 polymorphisms associated with modified p53 activity that share certain similarities with the absence of TIRR. For example, the P72R humanized mouse model is also metabolically impaired, but importantly, this effect is only present after exposure to an HFD.[36] This is a significant and critical difference from the current results. Additionally, the P72R model has a decreased overall lifespan despite a minor protection from malignancies, possibly because of excessive apoptosis.[37,38] This too represents a critically important difference between TIRR-mediated activity from these models. In order to strengthen our observations, we also performed analysis of RNA-seq data from hepatic samples of the $TIRR^{KO}$ mouse model and indeed found no significant differences in any of the genes regulated in the P72R model (Table S1). Therefore, TIRR suppression is evidently a novel way to activate p53 that affects metabolic balance under normal dietary conditions and protects against cancer without affecting overall lifespan. This unique model and approach open up new possibilities for exploring systems without relying on less physiological *in vitro* methods or potentially excessive external stimulation. This enables us to gain insights into a gene's function at the intersection of cancer and systemic metabolism more effectively. TIRR's absence in physiological conditions resulted in metabolic changes, without the need for external stimuli like an HFD or DNA-damaging agents. Unlike most other models, the trade-off between metabolic health and oncogenic protection observed in this study may stimulate additional studies to consider the link between systemic metabolism and cancer and the related mechanistic and therapeutic implications.

Taken together, we define TIRR as a crucial regulator of metabolism and oncogenesis by significantly controlling p53 function and an endogenous mechanism of reciprocation between systemic metabolic health and cancer with potential translational implications.

Limitations of the study

In this manuscript, we present compelling evidence indicating that TIRR loss results in cancer protection. However, we refrain from definitively stating whether this protection arises despite potential adverse effects on metabolic health or as their consequence. Additionally, we provide evidence that one of the pathways that could result in cancer protection is the suppression of the mevalonate pathway, acknowledging the possibility that oncoprotection might also arise from reduced LOH/LSTs due to TIRR loss. Finally, the suppression of the mevalonate pathway is not necessarily responsible for the metabolic abnormalities observed, which could be due to the increased inflammatory and cytokine pathways.

STAR★METHODS

RESOURCE AVAILABILITY

Lead contact—Further information and requests for resources and reagents should be directed to and will be fulfilled by the lead contact, Gökhan S. Hotamısxlıgil (ghotamis@hsph.harvard.edu).

Materials availability—All materials used in the analysis are available to any researcher for purposes of reproducing or extending the analysis.

Data and code availability

- RNA-seq data have been deposited at GEO and are publicly available as of the date of publication. Accession numbers are listed in the key resources table. All other data reported in this paper will be shared by the lead contact upon request.
- All original code has been deposited at Zenodo and is publicly available as of the date of publication. DOIs are listed in the key resources table.
- Any additional information required to reanalyze the data reported in this paper is available from the lead contact upon request.

EXPERIMENTAL MODEL AND STUDY PARTICIPANT DETAILS

Animal care and generation of mouse models—All animal procedures were conducted in compliance with protocols approved by IACUC and were in accordance with NIH guidelines. Mice were housed at 22°C–24°C using a 12h light/12h dark cycle. All mouse strains were on a C57B6 background, and littermate controls were used at all times. Animals were fed NCD (except in Figures S3B–S3I where they were fed an HFD, D12492: 60% kcal fat; Research Diets Inc.), had ad *libitum* access to water at all times, and food was only withdrawn if required for an experiment. For Dexa-scans the mice were anesthetized with isoflurane and bone mineral density, fat and, lean mass measurements were performed by the Dexa instrument (Piximus GE). $TIRR^{fl/wt}$ mice were generated by conditional gene targeting, flanking by *loxP* sites, of the first two exons of the TIRR gene in collaboration with Cyagen. We crossed the founder $TIRR^{fl/WT}$ (floxed/wild type) mice, already designed in a C57Bl6 background, to $EIIaCre^{TG/WT}$ (transgenic/wt) mice (also in a C57Bl6 background) to obtain litters with germline TIRR deletion (DEL).

EIIaCre$^{TG/WT}$;TIRR$^{DEL/WT}$ mice were subsequently crossed back to wildtype C57Bl6 mice, to eliminate the presence of the EIIaCre transgene, resulting in the generation of EIIaCre$^{WT/WT}$;TIRR$^{DEL/WT}$, or TIRR^{HET} mice (heterozygous for TIRR). TIRR^{HET} mice were intercrossed, and cohorts of littermate TIRR^{WT} and TIRR^{KO} (knockout) mice were generated. To obtain TIRR^{KO} mice, TIRR$^{fl/wt}$ mice were crossed to EIIaCre (Jax stock #003724) and after the generation of mice with germline deletion of the TIRR gene, the EIIaCre transgene was crossed out to avoid potential toxic effects of Cre expression in the whole body. TIRR^{KO} mice were born in Mendelian ratios, heterozygous breedings (TIRR^{HET} female x TIRR^{HET} male) resulted in 26% TIRR^{KO}, 50.4% TIRR^{HET} and 23.6% TIRR^{WT} mice. To generate B cell-specific TIRR deficient mice, TIRR$^{fl/fl}$ mice were bred to mice expressing Cre recombinase under the control of the CD19 promoter (CD19-Cre, Jax stock #006785). To generate adipocyte-specific TIRR deficient mice, TIRR$^{fl/fl}$ mice were bred to C57BL/6J mice expressing Cre recombinase under the control of the adiponectin promoter (Adp-Cre, Jax stock #028020). To generate CNS-specific TIRR deficient mice, TIRR$^{fl/fl}$ mice were bred to C57BL/6J mice expressing Cre recombinase under the control of the calcium/calmodulin-dependent protein kinase II alpha promoter which is expressed in the forebrain and the CA1 pyramidal cell layer of the hippocampus (Camk2a-Cre, Jax stock #005359). To generate p53^{KO};TIRR^{KO} mice, TIRR^{KO} mice were crossed to p53^{KO} obtained from Jax (stock #002101). Breedings with p53^{KO} mice yielded significantly less litters, therefore p53^{HET};TIRR^{WT} and p53^{HET};TIRR^{HET} mice were pooled and are referred to as p53^{HET};TIRR^{CONTROL}. Similarly, p53^{KO}; TIRR^{WT} and p53^{KO};TIRR^{HET} mice were pooled and are referred to as p53^{KO};TIRR^{CONTROL}. Tumor bearing mice were euthanized when the tumors reached a size of 2.0 cm in any dimension or if the tumors interfered with eating, drinking or ambulation, regardless of the size, or when they resulted in poor body condition, according to the guidelines of the DFCI animal research facility. 15% body weight loss was also endpoint for tumor-bearing mice. For the radiosensitivity experiment, 12- to 14-week-old female mice were irradiated and body weight and body conditioning score (BCS) were monitored daily for 28 days. Any animal showing weight loss equal to 15% from baseline or BCS = 8 was euthanized (body posture, eye appearance and activity level were used as indications for BCS). Body weight, insulin/glucose tolerance tests, body composition, and hormone measurements were performed in male mice, for consistency and to adhere to the principles of Reducing and Refining in the process of implementing a plethora of genetically modified models (as female mice were utilized for breeding, the radiosensitivity experiment, as well as lifespan experiments). For food intake measurements, the mice were single-caged with a special food hopper for 4 days, for acclimatization, prior to the two consecutive day measurements. Mice were genotyped either by tail or ear biopsy by Transnetyx.

Cell culture—For all *in vitro* experiments 3T3-L1 cells (ATCC) were seeded into culture dishes at approximately 70% confluence in DMEM with 4.5mM glucose (GIBCO) supplemented with 10% bovine calf serum (BCS) and 1% penicillin/streptomycin. For differentiation, once the cells reached 100% confluence (2–3 days after seeding), medium was changed to DMEM with 10% fetal bovine serum (FBS) with 1% penicillin/streptomycin. After 2 days (day 0), adipocyte differentiation was induced by the addition of 500 mM 3-isobutyl-1-methylxanthine (IBMX), 5 μg/mL insulin, 10 μM dexamethasone, and

10 μM rosiglitazone. On day 2 medium was switched to DMEM with 10% FBS and 1% penicillin/streptomycin, 5 μg/mL insulin and 10 μM rosiglitazone. On day 4, medium was switched to DMEM with 10% FBS and 1% penicillin/streptomycin (maintenance medium), and this medium was replaced every other day until day 10, when the adipocytes were fully differentiated. 10-day-diffentiated adipocytes were transfected with scramble or TIRR siRNA. For the transfection, cells were trypsinized (0.25% trypsin), transferred into 15 mL conical tubes and centrifuged for 10 min at 300 rpm at 4°C. The supernatant was removed, and the pellets were diluted in transfection media (DMEM, 10%FBS). The adipocytes were counted and seeded in 6 or 12-well plates (5×10^5 cells/well for 6-well plates and 2.5×10^5 cells/well for 12-well plates; at approximately 70% confluence). Lipofectamine-RNAiMax (Catalog #13778030) and Opti-MEM medium were from Thermo Fisher Scientific. Transfection mixtures were prepared following the lipofectamine-RNAiMAX-transfection protocol. The transfection mixture (300μl/well for 6-well plate) was added to the wells containing adipocytes, bringing the total volume of the wells up to 2.2 mL. The culture plates were incubated in 37°C incubators for 16 h. After 16 h, medium was replaced with maintenance medium and plates were incubated until 36 h after the transfection before performing the experiments. MEFs were isolated at embryonic day 13.5, immortalized by subsequent passaging and cultured in DMEM, 10% FBS.

Human samples from type-2 diabetic patients—The study on human patients was approved by the Bioethics Committee of the Medical University of Lodz (RNN/184/20/KE). Informed consent was obtained by all patients. All patients have been assessed with OGTT, HOMA-IR and fasting glucose prior to tissue collection. Human samples were obtained from visceral adipose tissue during bariatric surgery procedure (Roux-en-Y gastric bypass or laparoscopic gastric sleeve) performed at the Department of General Surgery, Medical University of Lodz, Poland. All participating patients were adults (>18 years old) with BMI over 35 kg/m^2 and were negative for pancreatic cancer. Tissues were stored in RNAlater and frozen at −80°C. RNA was isolated using RNeasy Lipid Tissue Mini Kit (QIAGEN) and RT-qPCR was performed for *NUDT16L1*.

METHOD DETAILS

Class switch recombination capacity—Primary spleen cells were isolated from wild type ($TIRR^{WT}$), heterozygous ($TIRR^{HET}$), whole-body TIRR ablation ($TIRR^{KO}$), $TIRR^{fl/fl}$ and B cell-specific TIRR ablation ($TIRR^{Bcell\ KO}$) mice. B cells were enriched by negative selection against CD43 which resulted in T cell removal from the cell suspension. Isolated primary B cells were cultured for 72 h in the presence of IL4 (Catalog #404-ML-010; R&D systems) and antiCD40 (Clone HM40–3, Catalog #14-0402-82; Invitrogen) in order to induce class switch recombination from IgM to IgG1. Class switching efficiency was assessed by fluorescence-activated cell sorting after B cells were immunohistochemically stained against B220 (PE Rat anti-mouse CD45R-B220 clone RA3–6B2 BD Catalog #561878; Pharmingen) and IgG1 (FITC Rat anti-mouse IgG1 BD Catalog #553443; Pharmingen). Data were analyzed by FlowJo.

Blood parameters and tolerance tests—Blood analysis was performed in cardiac blood after euthanasia, metabolic parameters were measured by Piccolo lipid panel plus

(Fisher Scientific, Catalog #07-P02-12A). Serum insulin was evaluated using ultrasensitive mouse insulin ELISA (Crystal Chem, USA) according to the manufacturer's protocol. For insulin tolerance tests, insulin was injected intraperitoneally (0.75U/kg) 1h after food withdrawal and blood glucose levels were measured throughout 60 min as indicated in the figures. For glucose tolerance tests, mice were administered glucose intraperitoneally after 6h fasting (lean: 2 g/kg, HFD-fed 1 g/kg), and blood glucose levels were measured throughout 120 min as indicated in the figures.

Histological analysis—For histological analysis, PGAT was fixed in 10% zinc-formalin for 24 h at room temperature and transferred to 70% ethanol for further storage. Tissues were processed, sectioned and stained with hematoxylin and eosin at the Histopathology facility at Harvard Medical School.

Gene expression analysis—RNA was isolated with Qiagen RNeasy lipid tissue kit for adipose tissue samples according to the manufacturers protocol, all other samples were isolated with Qiagen RNeasy kit. Quantitative real-time PCR reactions were performed in triplicates on a ViiA7 system (Applied Biosystems) using SYBR green and primer sets based on the Harvard primer bank. Gene of interest cycle thresholds (Cts) were normalized to housekeeping gene levels (as indicated on the figures) by the ΔΔCt method.

RNA-seq sample preparation and analysis—Procedures for RNA preparation, library construction and sequencing on the BGISEQ-500 platform have been described in detail previously.[18] For each sample, approximately 200ng of total RNA was enriched for poly-A RNA, fragmented into 200 to 300 bases, and converted to double-stranded cDNA libraries. Samples were then sequenced following the manufacturer's instructions to generate paired-end reads of 100-bases. Raw data with adapter sequences or low-quality sequences were filtered using SOAPnuke software with filter parameters "-n 0.03 -L 20 -q 0.4 -A 0.28". After base calling FASTQ files were preprocessed with fastp version 0.20.1 and next aligned to the mouse reference genome (GRCm39) with HISAT version 2.1.0. The standard alignment protocol was followed, with mus musculus Ensembl version 104 GTF annotation file. Read counts were analyzed using featureCounts version 2.0.1. The counts were normalized to the trimmed mean of M values (TMM) as implemented in the edgeR 3.12 package. Genes symbols were re-mapped using Ensembl BioMart from GRCm39 gene names to orthologous human (GRCh38.p13) gene names to allow the direct use of KEGG pathways from the molecular signatures database.

Gene set enrichment, modules and network analysis—Gene Set Enrichment Analysis (GSEA) was performed with GSEA Broad software version 4.1.0 using a collection of all canonical pathways from KEGG and REACTOME included in curated gene sets canonical pathways (C2) in MSigDB and manually added thermogenesis KEGG pathway (hsa04714) and p53 target gene set.[18] GSEA was performed using default settings. Gene sets were identified as significant if NOM p-value <0.05 and FDR<0.15. FDR cut-off of 0.15 was selected to provide more restricted than standard (FDR<0.25) approach, but not too restrictive to avoid increase the false-negative detection rate. To allow for multiple

GSEA enrichment plots display on a single graph, gseapy and matplotlib Python libraries were used.

TIRR's cancer-protective function in human cancers with heterozygous p53 loss—We investigated if low TIRR expression correlates with increased survival in primary lung adenocarcinoma patients. For that, we queried the GDC database for p53 mutated TCGA-LUAD, patients who reached remission and were prospectively monitored for relapses (date of access: 08/31/2021).[26] Data on mutations, translocation and copy number events in TCGA lung adenocarcinoma (LUAD) cases were collected from Broad GDAC Firehose data repository. Clinical data was accessed from GDC Pan-Cancer Clinical Data Resource.[39] From all LUAD samples ($N = 522$), summarized genomic data was available for 507 (97.13%) cases, of which 317 (62.52%) reached remission defined as complete or partial remission CR/PR by the RECIST criteria and were prospectively monitored for relapses. From those 317 cases, TP53 status was manually evaluated, resulting in 90 (28.39%) samples defined as *TP53* knock-out ($p53^{KO}$; deep homozygous deletion or single allele loss with concurrent loss-of-function dominant negative variant) and 60 (18.92%) as *TP53* heterozygous ($p53^{HET}$; single allele loss). From those patients, we extracted Transcriptome Profiling, Copy Number Variation and Clinical Data. RNAseq data for LUAD primary cancer tissue samples was preprocessed using biomaRt and edgeR, starting from HTSeq-Count counts and finishing on TMM-normalized gene expression. Progression-free survival by low/high TIRR (*NUDT16L1*), or p53-dependent signature gene, expression (below/above median) was evaluated using Kaplan-Meier curves and log rank test. As surrogate for TIRR knock-out, we also utilized single sample gene-set expression analysis (with the method as described further) for PGAT-derived p53-dependent signature and compared it against TIRR expression.

TIRR expression impact on pan-cancer progression-free survival in p53-dependent context—We investigated if low TIRR expression is associated with increased survival or longer time until cancer progression in multiple p53-proficient cancers. We manually selected samples with $p53^{HET}$ and $p53^{KO}$ status based on previously defined criteria. Paired clinical (GDC Pan-Cancer Clinical Data Resource[39]) and *NUDT16L1* expression data (Z score gene expression compared to all tissues, cBio-Portal) was available for 583 $p53^{HET}$ and 1325 $p53^{KO}$ samples. We defined criteria for inclusion of cancer cohort to the analysis as: complete or partial response reported for the first line of treatment, at least 10 records including 3 complete observations, with available progression-free survival status and time-to-event data. Resulting dataset consisted of 15 cancer types (BLCA, CESC, COAD, READ, ESCA, HNSC, LUAD, LUSC, OV, PAAD, PCPG, PRAD, STAD, UCEC and UCS) providing altogether 181 $p53^{HET}$ and 480 $p53^{KO}$ patient cases. Using collected data, we performed stratified Cox's regression analysis using cancer type as strata. This allowed us to determine effect of *NUDT16L1* on risk of progression.

Signature of transcriptomic changes associated with TIRR ablation—We further investigated similarities in the transcriptomic effects of whole-body and adipose tissue-specific TIRR ablation models. To this end, we determined genesets that were consistently and significantly regulated within perigonadal (PGAT) adipose tissue. We performed

leading-edge analysis (LEA) to determine common transcriptional changes associated with TIRR knockout (whole-body and adipose-specific) in PGAT tissues. The resulting genes were merged into a geneset associated with TIRR knockout in PGAT tissue.

p53-dependent transcriptomic signature of TIRR ablation—Similarly, we attempted to determine the impact of p53 on the transcriptomic changes associated with TIRR ablation. To this point, we utilized RNA-seq data from MEFs of the TIRR and P53 knock-out models. Such setup allowed us to determine transcriptomic changes that remained after p53 knock-out (p53-independent) and those that were affected by p53 ablation and for which initial regulation by TIRR ablation was either lost or reversed (p53-dependent). Using leading edge analysis, we determined gene lists for MEFs-derived p53-dependent and p53-independent TIRR ablation signatures. At this step, to avoid random discarding of genes, we applied pathway-level analysis of gene expression using singular value decomposition (PLAGE) and determined genes most associated with the expression of TIRR. PLAGE was performed on PGAT and genes with Pearson's absolute R coefficient >0.4 (strong correlation), and FDR<0.15 were selected for the p53-dependent and p53-independent signatures.

MEFs-derived signature of TIRR activation is conserved in $p53^{HET}$ lung adenocarcinoma patients in normal and cancer tissue samples, but not in $p53^{KO}$—Cancer transformation is associated with complex transcriptional changes. To confirm, that independently of cancer status, processes associated with TIRR are at least partially conserved and regulated by TIRR expression, we acquired TCGA LUAD mRNA-seq data for all available LUAD normal solid tissue – altogether 58 cases were found with available mRNA-seq data and no germline pathogenic variants or negative copy-number events in the genes of interest (TP53, TP53BP1). RNA-seq data preprocessing was performed as previously described, and TMM-normalized gene expression was used for computation of MEFs-derived signature of TIRR activation using ssGSEA. To determine the effect of cancer transformation, primary cancer tissue mRNA-seq data was obtained from GDC for patients with $p53^{HET}$ and $p53^{KO}$ tumor status. $p53^{HET}$ was defined as one wildtype and one lost p53 allele. Due to small number of double allele loss in cancer samples, we defined $p53^{KO}$ as loss of both p53 alleles (deep homodeletion) or loss of single allele with concurrent loss-of-function (LOF) dominant negative coding-region variant. Variants classified as LOF were accessed from the TP53 database (R20, July 2019).[40] We selected variants that had estimated effect of decreased transcriptional activity (≤20 score using method by Kato et al. 2003),[41] functional loss of growth-suppression and dominant-negative activity (DNE_LOF ≥0.61 and Etoposide Z score ≤ −0.21 using method by Giacomelli et al. 2018[42]).

Altogether, 60 $p53^{HET}$ and 107 $p53^{KO}$ primary cancer tissue samples were selected. mRNA-seq data was obtained from GDC and preprocessed as previously described to TMM-normalized gene expression and PGAT-derived signatures of TIRR ablation (general signature, p53-dependent and p53-independent) using ssGSEA. To determine the relationship between MEFs-derived signatures of TIRR ablation and TIRR expression (TMM-normalized) in normal solid tissue, $p53^{HET}$ and $p53^{KO}$ primary cancer tissue,

robust linear regression and Pearson's correlation tests were used. We observed that for p53-independent signature, $p53^{HET}$ and $p53^{KO}$ primary cancer tissues provided a strong and significant correlation with TIRR expression, which was conserved for $p53^{HET}$ but lost in $p53^{KO}$ in the p53-dependent signature.

Chromatin immunoprecipitation (ChIP) analysis—ChIP was performed as previously described.[18] Briefly, crosslinked cells were sonicated and diluted 10-fold with ChIP dilution buffer, and then incubated with protein A and protein G dynabeads (1:1 mix) and anti-p53 primary antibody (CatLog: P53-CM5P-L, Leica) at 4°C overnight. Antibody bound DNA was subsequently washed with low salt wash buffer, high salt wash buffer, LiCl wash buffer once, respectively, and then TE wash buffer twice. ChIPed DNA was reverse-crosslinked and purified ChIP-qPCR analysis. Primers used for ChIP-qPCR are: Abca1_FWD: 5′-GAC CCC GGA GTC GAA CAA AG-3'; Abca1_REV: 5′-GGA AGT GTC CTA AAC GGG GT-3'; Sqle_FWD: 5′-ACT CTG GTT ACT GTC CGC GA-3'; Sqle_REV: 5′-CTC GGA TGA GCG TCC TTC AG-3'.

***In silico* Pan-cancer TCGA analysis for TIRR's role on genomic stability—**We investigated the correlation between TIRR expression and genomic stability, using as measures the loss of heterozygosity (LOH) and large-scale transitions (LST). Scores were accessed from Marquard et al. supplementary data and cross-referenced with mutational, translocation and copy number events as provided by Broad GDAC Firehose data repository. Altogether, 4358 entries were collected and evaluated for defects in DDR pathways with core genes of interest defined after Knijnenburg et al. (LIG4, NHEJ1, POLL, POLM, PRKDC, XRCC4, XRCC5, XRCC6, BARD1, BLM, BRCA1, BRCA2, BRIP1, EME1, GEN1, MRE11A, MUS81, NBN, PALB2, RAD50, RAD51, RAD52, RBBP8, SHFM1, SLX1A, TOP3A, TP53BP1, XRCC2, XRCC3 and we additionally added TP53BP1, TP53 and NUDT16L1 -TIRR-as genes of interest). From 4358 entries, 2066 were marked as functional -defined as harboring no pathogenic mutations and having at least one wildtype allele of each gene of interest (in case of gene-level or exon-level copy number alternation)-. From all entries, we selected as functional and analyzed the following 34/141 of all STAD, 91/283 of all LUAD, 209/310 of all PRAD and 51/238 of all ovarian cancers. Batch normalized NUDT16L1 and TP53BP1 mRNA expression was obtained from cBioPortal (date of access: 09/30/2021) and correlated with LOH and LST scores using Pearson correlation.

QUANTIFICATION AND STATISTICAL ANALYSIS

Data analysis of the metabolic experiments was performed with Graphpad Prism (Graphpad Software Inc., La Jolla, CA, USA). Numerical values were given as mean ± standard error. To determine differences in means t tests and two-way ANOVA tests were performed. A significance level of 0.05 was accepted for all tests. $*p \leq 0.05$; $**p \leq 0.01$; $***p \leq 0.001$ versus controls.

All the statistical analysis of the RNAseq data was performed in Python, version 3.7.10 (www.python.org), with pandas, numpy, scipy, statsmodels, sklearn and umap libraries for the numerical computation and matplotlib, and seaborn for the visualization. Data were

visualized in 2-dimensional scatterplots after dimensionality reduction using PCA (between-tissues) and PCA (within-tissue). Differential expression (DE) was performed using a t test for independent samples with Benjamini-Hochberg multiple testing adjustment procedure.

Supplementary Material

Refer to Web version on PubMed Central for supplementary material.

ACKNOWLEDGMENTS

This work is supported by the Hotamısxlıgil Lab and Sabri Ülker Center for Metabolic Research. E.T. was supported by an AHA postdoctoral fellowship (18POST33990109). W.F. and J.C. were supported by the Foundation for Polish Science grant First TEAM/2016–2/11. J.C. was supported by the Ministry of Education and Science (Poland) grant “Pearls of Science,” project number PN/01/0025/2022. E.G. was supported by a T32 Ruth L. Kirschstein National Research Service Award (5 T32 CA 151022–13). D.C. is supported by R01 CA208244 and R01 CA264900, the Gray Foundation Team Science Award, DOD Ovarian Cancer Award W81XWH-15-0564/OC140632, Tina’s Wish Foundation, the V Foundation Award, and Detect Me if You Can. Portions of the graphical abstract utilized images from Servier Medical Art, licensed under a Creative Commons attribution 3.0 unported license. Special thanks to Dr. Karen Inouye for support with the *in vivo* animal research protocols at the Sabri Ülker Center and the rest of the Hotamısxlıgil laboratory for their encouragement.

REFERENCES

1. De Pergola G, and Silvestris F (2013). Obesity as a Major Risk Factor for Cancer. J. Obes. 2013, 291546–291611. 10.1155/2013/291546. [PubMed: 24073332]
2. White MC, Holman DM, Boehm JE, Peipins LA, Grossman M, and Henley SJ (2014). Age and cancer risk: a potentially modifiable relationship. Am. J. Prev. Med. 46, S7–S15. 10.1016/j.amepre.2013.10.029. [PubMed: 24512933]
3. DeBerardinis RJ, and Chandel NS (2016). Fundamentals of cancer metabolism. Sci. Adv. 2, e1600200. 10.1126/sciadv.1600200. [PubMed: 27386546]
4. Anderson NM, and Simon MC (2020). The tumor microenvironment. Curr. Biol. 30, R921–R925. 10.1016/j.cub.2020.06.081. [PubMed: 32810447]
5. Levine AJ, and Puzio-Kuter AM (2010). The Control of the Metabolic Switch in Cancers by Oncogenes and Tumor Suppressor Genes. Science 330, 1340–1344. 10.1126/science.1193494. [PubMed: 21127244]
6. Shimizu I, Yoshida Y, Suda M, and Minamino T (2014). DNA Damage Response and Metabolic Disease. Cell Metabol. 20, 967–977. 10.1016/j.cmet.2014.10.008.
7. Arruda AP, and Hotamisligil GS (2015). Calcium Homeostasis and Organelle Function in the Pathogenesis of Obesity and Diabetes. Cell Metabol. 22, 381–397. 10.1016/j.cmet.2015.06.010.
8. García-Cao I, García-Cao M, Martín-Caballero J, Criado LM, Klatt P, Flores JM, Weill J-C, Blasco MA, and Serrano M (2002). “Super p53” mice exhibit enhanced DNA damage response, are tumor resistant and age normally. EMBO J. 21, 6225–6235. 10.1093/emboj/cdf595. [PubMed: 12426394]
9. Tyner SD, Venkatachalam S, Choi J, Jones S, Ghebranious N, Igelmann H, Lu X, Soron G, Cooper B, Brayton C, et al. (2002). p53 mutant mice that display early ageing-associated phenotypes. Nature 415, 45–53. 10.1038/415045a. [PubMed: 11780111]
10. Montes de Oca Luna R, Wagner DS, and Lozano G (1995). Rescue of early embryonic lethality in mdm2-deficient mice by deletion of p53. Nature 378, 203–206. 10.1038/378203a0. [PubMed: 7477326]
11. Jones SN, Roe AE, Donehower LA, and Bradley A (1995). Rescue of embryonic lethality in Mdm2-deficient mice by absence of p53. Nature 378, 206–208. 10.1038/378206a0. [PubMed: 7477327]
12. Parant J, Chavez-Reyes A, Little NA, Yan W, Reinke V, Jochemsen AG, and Lozano G (2001). Rescue of embryonic lethality in Mdm4-null mice by loss of Trp53 suggests a nonoverlapping pathway with MDM2 to regulate p53. Nat. Genet. 29, 92–95. 10.1038/ng714. [PubMed: 11528400]

13. Minamino T, Orimo M, Shimizu I, Kunieda T, Yokoyama M, Ito T, Nojima A, Nabetani A, Oike Y, Matsubara H, et al. (2009). A crucial role for adipose tissue p53 in the regulation of insulin resistance. Nat. Med. 15, 1082–1087. 10.1038/nm.2014. [PubMed: 19718037]

14. Drané P, Brault M-E, Cui G, Meghani K, Chaubey S, Detappe A, Parnandi N, He Y, Zheng X-F, Botuyan MV, et al. (2017). TIRR regulates 53BP1 by masking its histone methyl-lysine binding function. Nature 543, 211–216. 10.1038/nature21358. [PubMed: 28241136]

15. Botuyan MV, Cui G, Drané P, Oliveira C, Detappe A, Brault ME, Parnandi N, Chaubey S, Thompson JR, Bragantini B, et al. (2018). Mechanism of 53BP1 activity regulation by RNA-binding TIRR and a designer protein. Nat. Struct. Mol. Biol. 25, 591–600. 10.1038/s41594-018-0083-z. [PubMed: 29967538]

16. Mirman Z, and de Lange T (2020). 53BP1: a DSB escort. Genes Dev. 34, 7–23. 10.1101/gad.333237.119. [PubMed: 31896689]

17. Durocher D, and Pelletier L (2016). 53BP1 Goes Back to Its p53 Roots. Mol. Cell 64, 3–4. 10.1016/j.molcel.2016.09.024. [PubMed: 27716486]

18. Parnandi N, Rendo V, Cui G, Botuyan MV, Remisova M, Nguyen H, Drané P, Beroukhim R, Altmeyer M, Mer G, and Chowdhury D (2021). TIRR inhibits the 53BP1-p53 complex to alter cell-fate programs. Mol. Cell 81, 2583–2595.e6. 10.1016/j.molcel.2021.03.039. [PubMed: 33961797]

19. Ward IM, Reina-San-Martin B, Olaru A, Minn K, Tamada K, Lau JS, Cascalho M, Chen L, Nussenzweig A, Livak F, et al. (2004). 53BP1 is required for class switch recombination. J. Cell Biol. 165, 459–464. 10.1083/jcb.200403021. [PubMed: 15159415]

20. Vergoni B, Cornejo P-J, Gilleron J, Djedaini M, Ceppo F, Jacquel A, Bouget G, Ginet C, Gonzalez T, Maillet J, et al. (2016). DNA Damage and the Activation of the p53 Pathway Mediate Alterations in Metabolic and Secretory Functions of Adipocytes. Diabetes 65, 3062–3074. 10.2337/db16-0014. [PubMed: 27388216]

21. Hardy OT, Perugini RA, Nicoloro SM, Gallagher-Dorval K, Puri V, Straubhaar J, and Czech MP (2011). Body mass index-independent inflammation in omental adipose tissue associated with insulin resistance in morbid obesity. Surg. Obes. Relat. Dis. 7, 60–67. 10.1016/j.soard.2010.05.013. [PubMed: 20678967]

22. Hotamisligil GS (2017). Inflammation, metaflammation and immunometabolic disorders. Nature 542, 177–185. 10.1038/nature21363. [PubMed: 28179656]

23. Moon S-H, Huang C-H, Houlihan SL, Regunath K, Freed-Pastor WA, Morris JP, Tschaharganeh DF, Kastenhuber ER, Barsotti AM, Culp-Hill R, et al. (2019). p53 Represses the Mevalonate Pathway to Mediate Tumor Suppression. Cell 176, 564–580.e19. 10.1016/j.cell.2018.11.011. [PubMed: 30580964]

24. Tsaousidou E, Paeger L, Belgardt BF, Pal M, Wunderlich CM, Brönneke H, Collienne U, Hampel B, Wunderlich FT, SchmidtSupprian M, et al. (2014). Distinct Roles for JNK and IKK Activation in Agouti-Related Peptide Neurons in the Development of Obesity and Insulin Resistance. Cell Rep. 9, 1495–1506. 10.1016/j.celrep.2014.10.045. [PubMed: 25456138]

25. Jacks T, Remington L, Williams BO, Schmitt EM, Halachmi S, Bronson RT, and Weinberg RA (1994). Tumor spectrum analysis in p53-mutant mice. Curr. Biol. 4, 1–7. 10.1016/S09609822(00)00002-6. [PubMed: 7922305]

26. Grossman RL, Heath AP, Ferretti V, Varmus HE, Lowy DR, Kibbe WA, and Staudt LM (2016). Toward a Shared Vision for Cancer Genomic Data. N. Engl. J. Med. 375, 1109–1112. 10.1056/NEJMp1607591. [PubMed: 27653561]

27. Sun H, Li L, Li W, Yang F, Zhang Z, Liu Z, and Du W (2021). p53 transcriptionally regulates SQLE to repress cholesterol synthesis and tumor growth. EMBO Rep. 22, e52537. 10.15252/embr.202152537. [PubMed: 34459531]

28. Dai Y, Zhang A, Shan S, Gong Z, and Zhou Z (2018). Structural basis for recognition of 53BP1 tandem Tudor domain by TIRR. Nat. Commun. 9, 2123. 10.1038/s41467-018-04557-2. [PubMed: 29844495]

29. Wang J, Yuan Z, Cui Y, Xie R, Yang G, Kassab MA, Wang M, Ma Y, Wu C, Yu X, and Liu X (2018). Molecular basis for the inhibition of the methyl-lysine binding function of 53BP1 by TIRR. Nat. Commun. 9, 2689. 10.1038/s41467-018-05174-9. [PubMed: 30002377]

30. Matheu A, Maraver A, Klatt P, Flores I, Garcia-Cao I, Borras C, Flores JM, Viña J, Blasco MA, and Serrano M (2007). Delayed ageing through damage protection by the Arf/p53 pathway. Nature 448, 375–379. 10.1038/nature05949. [PubMed: 17637672]

31. Sanz G, Singh M, Peuget S, and Selivanova G (2019). Inhibition of p53 inhibitors: progress, challenges and perspectives. J. Mol. Cell Biol. 11, 586–599. 10.1093/jmcb/mjz075.

32. Konopleva M, Martinelli G, Daver N, Papayannidis C, Wei A, Higgins B, Ott M, Mascarenhas J, and Andreeff M (2020). MDM2 inhibition: an important step forward in cancer therapy. Leukemia 34, 2858–2874. 10.1038/s41375-020-0949-z. [PubMed: 32651541]

33. Mendrysa SM, McElwee MK, Michalowski J, O'Leary KA, Young KM, and Perry ME (2003). mdm2 Is Critical for Inhibition of p53 during Lymphopoiesis and the Response to Ionizing Irradiation. MCB 23, 462–472. 10.1128/MCB.23.2.462-473.2003. [PubMed: 12509446]

34. Terzian T, Wang Y, Van Pelt CS, Box NF, Travis EL, and Lozano G (2007). Haploinsufficiency of Mdm2 and Mdm4 in Tumorigenesis and Development. MCB 27, 5479–5485. 10.1128/MCB.00555-06. [PubMed: 17526734]

35. Nguyen T-AT, Grimm SA, Bushel PR, Li J, Li Y, Bennett BD, Lavender CA, Ward JM, Fargo DC, Anderson CW, et al. (2018). Revealing a human p53 universe. Nucleic Acids Res. 46, 8153–8167. 10.1093/nar/gky720. [PubMed: 30107566]

36. Kung C-P, Leu JI-J, Basu S, Khaku S, Anokye-Danso F, Liu Q, George DL, Ahima RS, and Murphy ME (2016). The P72R Polymorphism of p53 Predisposes to Obesity and Metabolic Dysfunction. Cell Rep. 14, 2413–2425. 10.1016/j.celrep.2016.02.037. [PubMed: 26947067]

37. Hasty P, Campisi J, and Sharp ZD (2016). Do p53 stress responses impact organismal aging? Transl. Cancer Res. 5, 685–691. 10.21037/tcr.2016.12.02. [PubMed: 30984573]

38. Zhao Y, Wu L, Yue X, Zhang C, Wang J, Li J, Sun X, Zhu Y, Feng Z, and Hu W (2018). A polymorphism in the tumor suppressor p53 affects aging and longevity in mouse models. Elife 7, e34701. 10.7554/eLife.34701. [PubMed: 29557783]

39. Liu J, Lichtenberg T, Hoadley KA, Poisson LM, Lazar AJ, Cherniack AD, Kovatich AJ, Benz CC, Levine DA, Lee AV, et al. (2018). An Integrated TCGA Pan-Cancer Clinical Data Resource to Drive High-Quality Survival Outcome Analytics. Cell 173, 400–416.e11. 10.1016/j.cell.2018.02.052. [PubMed: 29625055]

40. de Andrade KC, Lee EE, Tookmanian EM, Kesserwan CA, Manfredi JJ, Hatton JN, Loukissas JK, Zavadil J, Zhou L, Olivier M, et al. (2022). The TP53 Database: transition from the International Agency for Research on Cancer to the US National Cancer Institute. Cell Death Differ. 29, 1071–1073. 10.1038/s41418-022-00976-3. [PubMed: 35352025]

41. Kato S, Han S-Y, Liu W, Otsuka K, Shibata H, Kanamaru R, and Ishioka C (2003). Understanding the function-structure and function-mutation relationships of p53 tumor suppressor protein by high-resolution missense mutation analysis. Proc. Natl. Acad. Sci. USA 100, 8424–8429. 10.1073/pnas.1431692100. [PubMed: 12826609]

42. Giacomelli AO, Yang X, Lintner RE, McFarland JM, Duby M, Kim J, Howard TP, Takeda DY, Ly SH, Kim E, et al. (2018). Mutational processes shape the landscape of TP53 mutations in human cancer. Nat. Genet. 50, 1381–1387. 10.1038/s41588-018-0204-y. [PubMed: 30224644]

Highlights

- TIRR, by inhibiting p53, has opposing roles in metabolic homeostasis and oncogenesis
- TIRR-deficient mice are spontaneously overweight and insulin resistant
- TIRR deletion improves $p53^{HET}$ mouse survival, and the oncoprotective effect is p53 dependent
- Low TIRR correlates with enhanced survival in patients with p53 heterozygous carcinomas

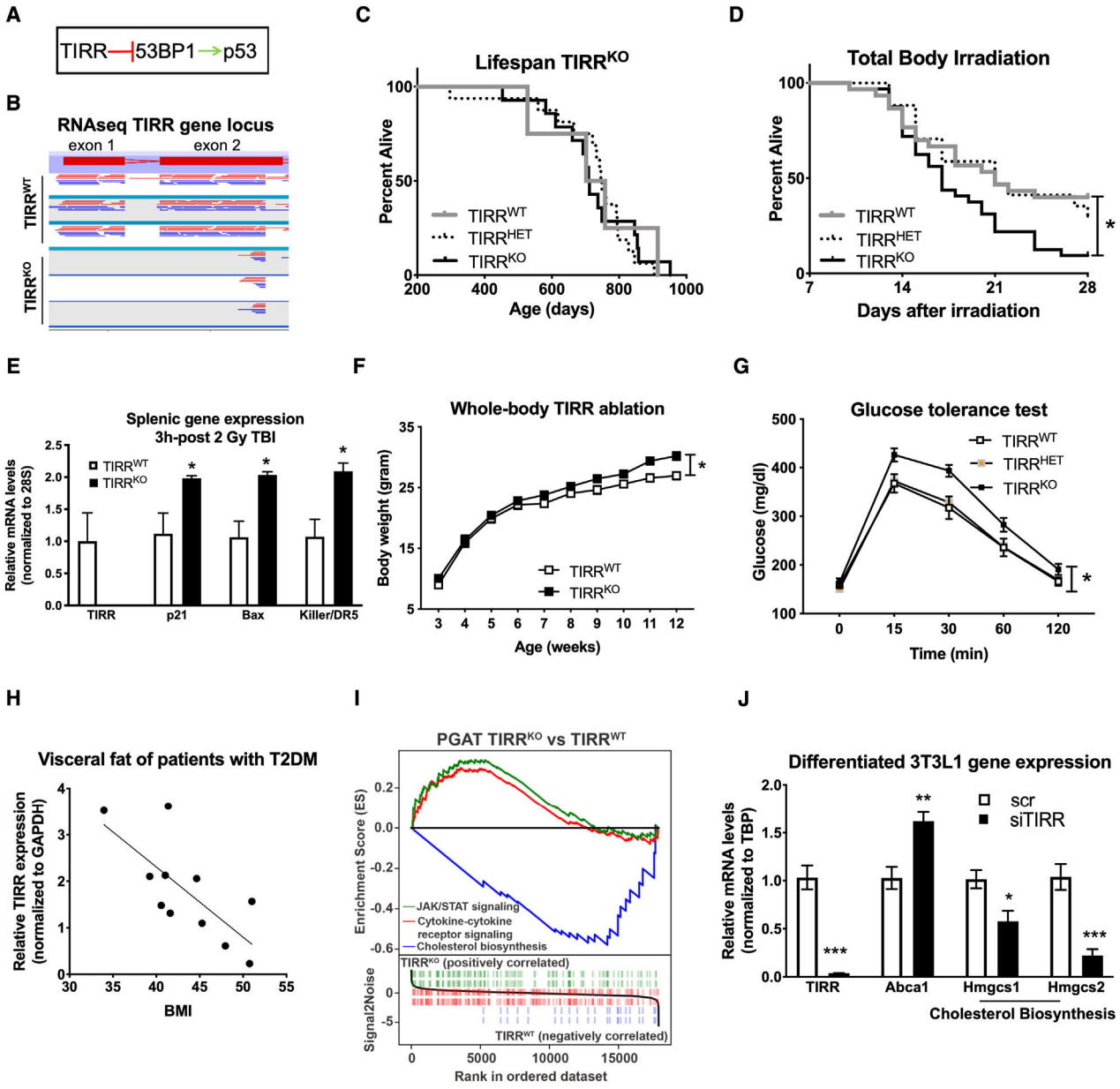

Figure 1. TIRR has a p53-dependent metabolic role

(A) TIRR is an inhibitor of the 53BP1/p53 complex.

(B) RNA-seq analysis reads in the region of the first two exons of the TIRR gene of TIRR^{WT} (n = 3) and TIRR^{KO} (n = 3) mice.

(C) Lifespan of TIRR^{WT} (n = 4), TIRR^{HET} (n = 16), and TIRR^{KO} (n = 14) mice is unchanged.

(D) Survival curves over 28 days of TIRR^{WT} (n = 30), TIRR^{HET} (n = 17), and TIRR^{KO} (n = 32) mice after exposure to 8.5 Gy total body irradiation (TBI). The 8.5 Gy dose was used, as we could achieve a 60% survival in the control group after 28 days (Figure S1K).

(E) Splenic gene expression of p53 target genes 3 h post-exposure to 2 Gy TBI of TIRR^{WT} (n = 3) and TIRR^{KO} (n = 3) mice.

(F) Body weight curves of male TIRR^{WT} (n = 7) and TIRR^{KO} (n = 11) mice fed NCD.

(G) Blood glucose concentrations during intraperitoneal glucose tolerance test of 13-week-old male $TIRR^{WT}$ ($n = 18$), $TIRR^{HET}$ ($n = 24$), and $TIRR^{KO}$ ($n = 24$) mice. Notably, $TIRR^{HET}$ mice have similar glucose tolerance to $TIRR^{WT}$.

(H) Linear regression between TIRR expression (normalized to GAPDH) and BMI from visceral adipose tissue of patients with type 2 diabetes mellitus (T2DM) ($n = 11$, $R = 0.73$, $p = 0.010$).

(I) GSEA of PGAT samples of $TIRR^{WT}$ ($n = 3$) against $TIRR^{KO}$ ($n = 4$) mice showing significant upregulation of the JAK/STAT signaling pathway in $TIRR^{KO}$ mice (normalized enrichment score [NES] = 1.700, $p = 0.003$, false discovery rate [FDR] = 0.026), significant upregulation of the cytokine-cytokine receptor signaling pathway in $TIRR^{KO}$ mice (NES = 1.720, $p < 0.001$, FDR = 0.023), and significant suppression of the cholesterol biosynthesis pathway in $TIRR^{KO}$ mice (NES = 1.9252, $p < 0.0001$, FDR = 0.010).

(J) Relative gene expression levels in differentiated 3T3L1 cells treated with scramble or siTIRR. Depicted are means and SEM, * $p < 0.05$, ** $p < 0.01$, and *** $p < 0.001$.

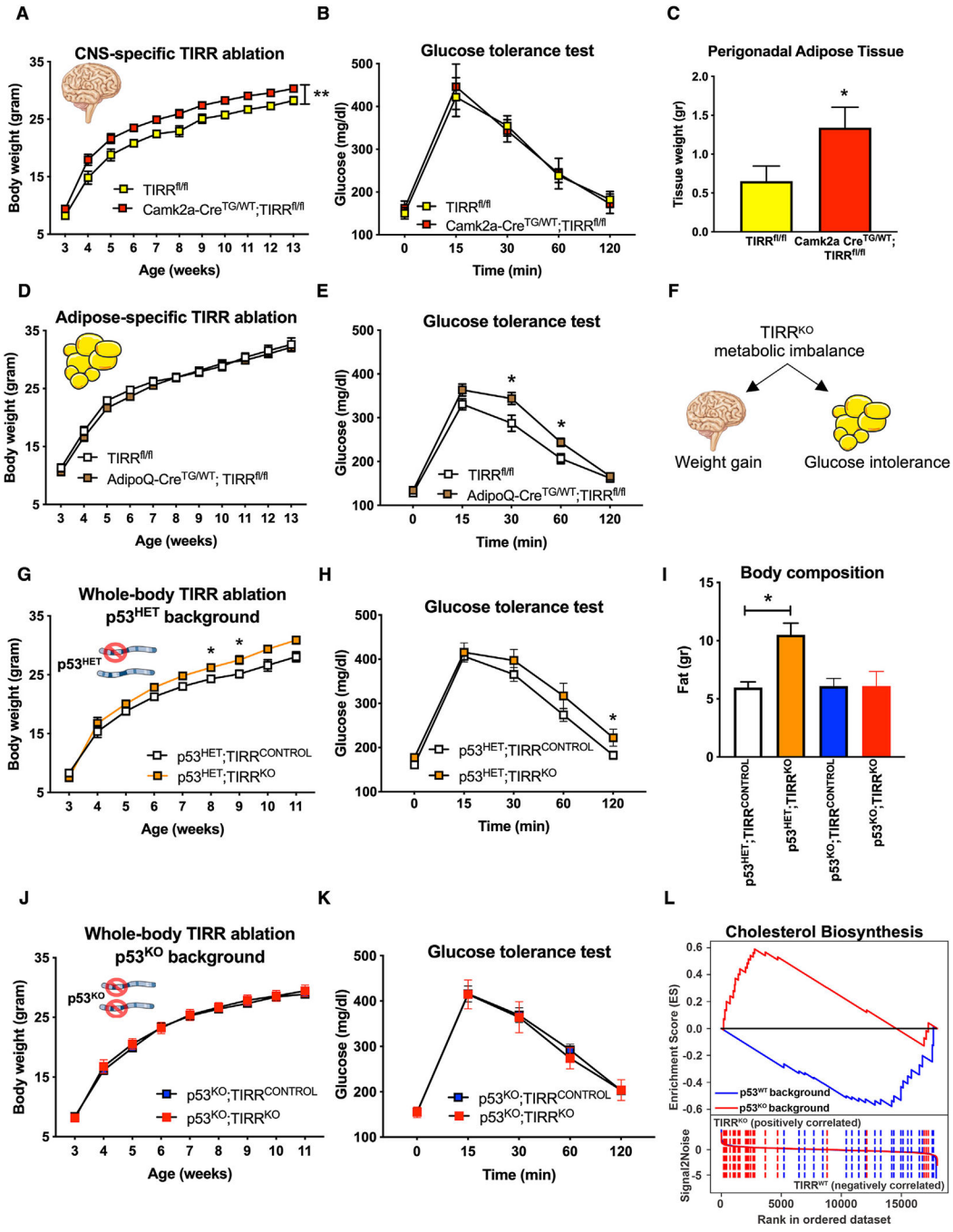

Figure 2. TIRR has tissue-specific roles in the regulation of body weight and glucose homeostasis

(A) Body weight curves of male TIRR$^{fl/fl}$ (n = 8) and Camk2a-Cre$^{TG/WT}$;TIRR$^{fl/fl}$ (n = 11) mice fed NCD.

(B) Blood glucose concentrations during intraperitoneal glucose tolerance test of 13-week-old male TIRR$^{fl/fl}$ (n = 5) and Camk2a-Cre$^{TG/WT}$;TIRR$^{fl/fl}$ (n = 4) mice fed NCD.

(C) PGAT weight of 17-week-old TIRR$^{fl/fl}$ (n = 4) and Camk2a-Cre$^{TG/WT}$;TIRR$^{fl/fl}$ (n = 3) mice.

(D) Body weight curves of male $TIRR^{fl/fl}$ ($n = 11$) and AdipoQ-$Cre^{TG/WT}$;$TIRR^{fl/fl}$ ($n = 17$) mice fed NCD.

(E) Blood glucose concentrations during intraperitoneal glucose tolerance test of 13-week-old male $TIRR^{fl/fl}$ ($n = 14$) and AdipoQ-$Cre^{TG/WT}$;$TIRR^{fl/fl}$ ($n = 20$) mice.

(F) CNS-specific TIRR ablation results in increased body weight and adipose-specific TIRR ablation in impaired glucose homeostasis.

(G) Body weight curves of male $p53^{HET}$;$TIRR^{CONTROL}$ ($n = 7–22$) and $p53^{HET}$;$TIRR^{KO}$ ($n = 3–9$) mice fed NCD.

(H) Blood glucose concentrations during intraperitoneal glucose tolerance test of 13-week-old male $p53^{HET}$;$TIRR^{CONTROL}$ ($n = 26$) and $p53^{HET}$;$TIRR^{KO}$ ($n = 10$) mice.

(I) DEXA-scan body composition measurement of the total fat mass of 17-week-old $p53^{HET}$;$TIRR^{CONTROL}$ ($n = 6$), $p53^{HET}$;$TIRR^{KO}$ ($n = 4$), $p53^{KO}$;$TIRR^{CONTROL}$ ($n = 5$), and $p53^{KO}$;$TIRR^{KO}$ ($n = 4$) mice.

(J) Body weight curves of male $p53^{KO}$;$TIRR^{CONTROL}$ ($n = 10–16$) and $p53^{KO}$;$TIRR^{KO}$ ($n = 4–7$) mice fed NCD.

(K) Blood glucose concentrations during intraperitoneal glucose tolerance test of 13-week-old male $p53^{KO}$;$TIRR^{CONTROL}$ ($n = 21$) and $p53^{KO}$;$TIRR^{KO}$ ($n = 7$) mice.

(L) GSEA of PGAT samples for cholesterol biosynthesis pathway in $TIRR^{KO}$ vs. $TIRR^{WT}$ mice in $p53^{WT}$ and $p53^{KO}$ backgrounds (NES = 1.925, $p < 0.001$, FDR = 0.010 and NES = 2.444, $p < 0.001$, FDR < 0.001, respectively). Depicted are means and SEM, * $p < 0.05$ and ** $p < 0.01$.

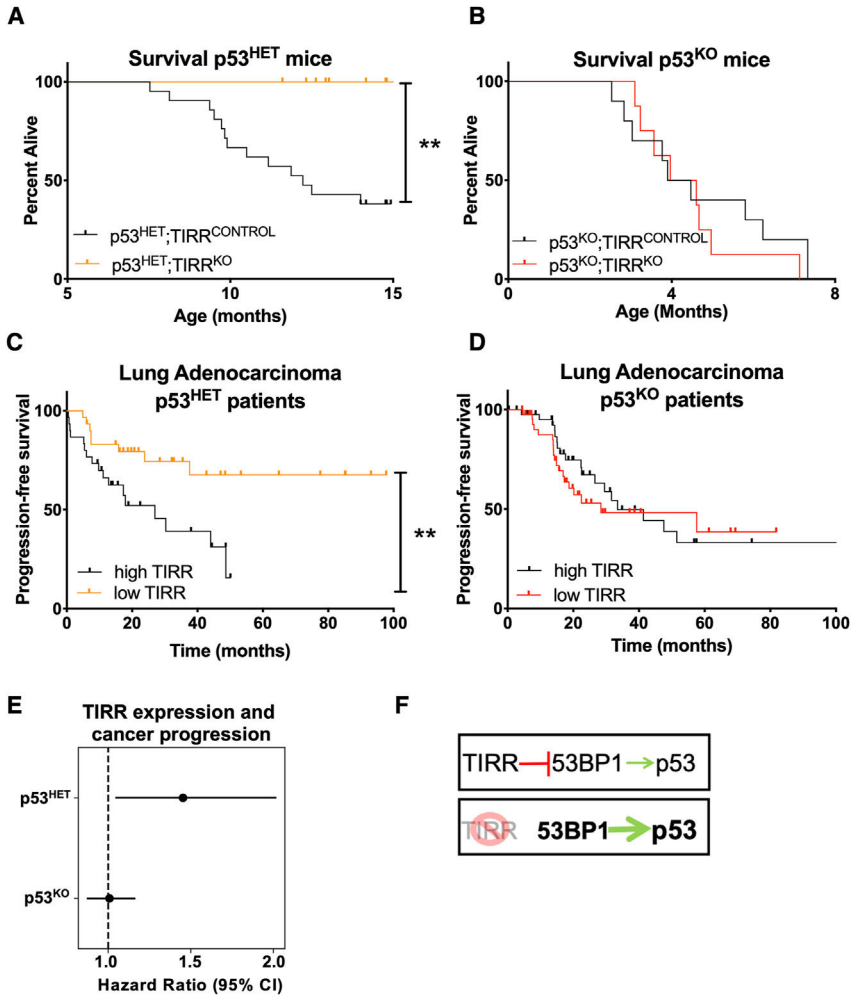

Figure 3. TIRR suppression mediates p53-dependent cancer prevention

(A) Kaplan-Meier plot demonstrating increased survival of $p53^{HET};TIRR^{KO}$ ($n = 11$) mice compared to $p53^{HET};TIRR^{CONTROL}$ ($n = 22$) littermate mice. The $p53^{HET};TIRR^{KO}$ mice had no incidence of cancer until the age of 15 months, whereas the $p53^{HET}$; $TIRR^{CONTROL}$ mice had a median survival of 12.2 months. 37% of the deceased $p53^{HET}$; $TIRR^{CONTROL}$ mice developed sarcomas and 26% of them developed lymphomas, with the rest presenting with different types of carcinomas. Log-rank (Mantel-Cox) test $p = 0.002$.

(B) Kaplan-Meier plot demonstrating similar survival($p = 0.52$) between $p53^{KO};TIRR^{CONTROL}$ ($n = 10$) and $p53^{KO};TIRR^{KO}$ ($n = 8$) littermate mice.

(C) Kaplan-Meier plot demonstrating PFS of $p53^{HET}$ patients after complete response or partial response treatment of primary LUAD (as defined by the median, high TIRR $n = 30$ and low TIRR $n = 30$, $p = 0.002$).

(D) Kaplan-Meier plot demonstrating PFS of p53deficient patients after complete response and partial response treatment of primary LUAD (as defined by the median, high TIRR $n =$ 45 and low TIRR $n = 45$).

(E) Forest plot for cancer progression against TIRR expression for $p53^{HET}$ ($n = 181$) and $p53^{KO}$ ($n = 480$) cancers (stratified Cox's regression).

(F) Graphical representation of TIRR's role as an indirect inhibitor of p53.

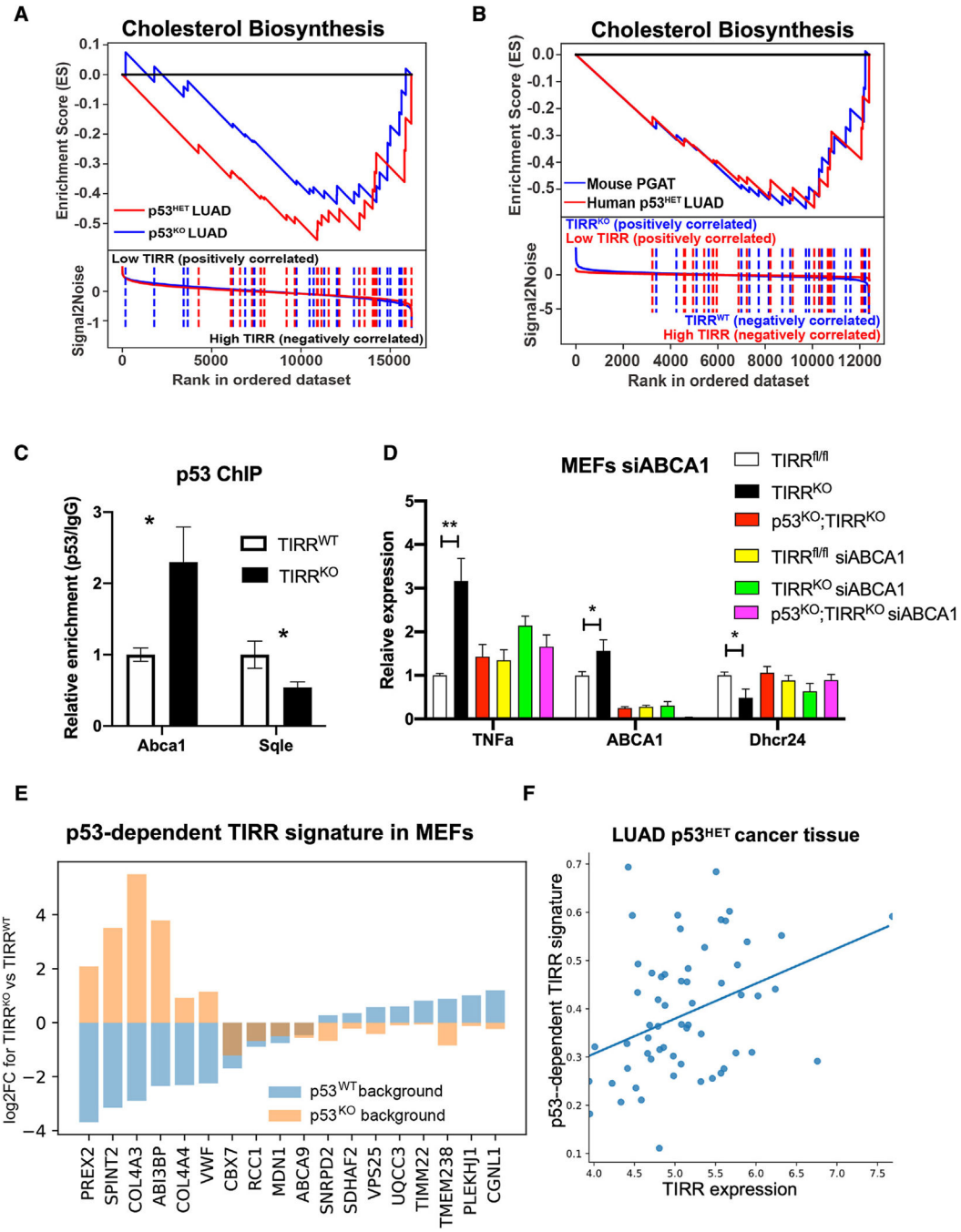

Figure 4. Identification of a p53-dependent TIRR-specific transcriptomic signature with the potential to serve as a prognostic tool

(A) GSEA of mouse PGAT samples ($TIRR^{KO}$ vs. $TIRR^{WT}$, NES = −1.925, $p < 0.001$, FDR = 0.010) and $p53^{HET}$ LUAD samples of patients with high TIRR ($n = 30$) against low TIRR ($n = 30$) expression showing significant suppression of the cholesterol biosynthesis pathway in low-TIRR samples (NES = −1.819, $p = 0.004$, FDR = 0.017).

(B) GSEA overlap for cholesterol biosynthesis pathway from LUAD samples with high (above median) and low (below median) TIRR expression of $p53^{HET}$ (NES = −1.819, $p = 0.004$, FDR = 0.017) and $p53^{KO}$ (NES = 1.420, $p = -0.074$, FDR = 0.112) samples.

(C) ChIP-PCR revealed significant regulation of Abca1 and Sqle promoters by p53 in the absence of TIRR in MEFs.

(D) Relative gene expression levels of TNF-α, ABCA1, and Dhcr24 in MEFs treated with siABCA1.

(E) Log2 fold change (Log2FC) for p53-dependent $TIRR^{KO}$ signature derived from MEFs ($TIRR^{fl/fl}$, $TIRR^{KO}$, and $p53^{KO}$;$TIRR^{KO}$).

(F) p53-dependent TIRR signature score and TIRR expression (log2 value + 1) significantly correlate in cancer tissue of patients with primary $p53^{HET}$ LUAD (Pearson R = 0.34, $p = 0.007$). Depicted means are SEM, * $p < 0.05$ and **** $p < 0.0001$.

KEY RESOURCES TABLE

REAGENT or RESOURCE	SOURCE	IDENTIFIER
Antibodies		
anti-Abca1	Novus Biologicals	Cat# NB400–105; RRID: AB_10000630
anti-p53 primary antibody	Leica	Cat#P53-CM5P-L RRID: AB_563933
anti-phospho-p53 (Ser15) antibody	Cell Signaling	Cat#9284 RRID: AB_331464
anti-acetyl-p53 (Lys379) antibody	Cell Signaling	Cat#2570 RRID: AB_823591
Anti-Tubulin	Santa Cruz Biotechnology	Cat# sc-9104 RRID: AB_2241191
antiCD40 (Clone HM40–3)	Invitrogen	Cat#14–0402-82 RRID: AB_467228
anti-B220 (PE Rat anti-mouse CD45R-B220 clone RA3–6B2 BD)	Pharmingen	Cat#561878 RRID: AB_10893353
anti-IgG1 (FITC Rat anti-mouse IgG1 BD)	Pharmingen	Cat#553443 RRID: AB_394862
Biological samples		
Human visceral adipose tissue biopsies	This paper	N/A
Mouse tissues (perigonadal adipose tissue, liver, hypothalamus, spleen, quadriceps muscle)	This paper	N/A
Chemicals, peptides, and recombinant proteins		
Standard chow PicoLab Mouse Diet 20	LabDiet	Cat# 5058
HFD, 60% kcal fat	Research Diets Inc.	Cat#D12492
Dexa instrument	Piximus GE	N/A
Lipofectamine-RNAiMax	Thermo Fisher Scientific	Cat#13778030
IL4	R&D systems	Cat#404-ML-010
DMEM	GIBCO	Cat# 11965
3-isobutyl-1-methylxanthine (IBMX)	Sigma-Aldrich	Cat#I5879
dexamethasone	Sigma-Aldrich	Cat#D4902
rosiglitazone	Sigma-Aldrich	Cat#R2408
Opti-MEM	Thermo Fisher Scientific	Cat#31985070
Critical commercial assays		
Piccolo lipid panel plus	Fisher Scientific	Cat#07-P02–12A
Ultrasensitive mouse insulin ELISA	Crystal Chem, USA	Cat#90080
Adiponectin ELISA	Crystal Chem, USA	Cat#80569
Leptin ELISA	Crystal Chem, USA	Cat#90030
Deposited data		
RNA-seq data	This paper	GSE210900https://www.ncbi.nlm.nih.gov/geo/query/acc.cgi?acc=GSE210900
Raw data	This paper	Mendeley Data:http://www.doi.org/10.17632/yvhn4hn3b8.1
Original code	This paper	https://zenodo.org/records/6904028

REAGENT or RESOURCE	SOURCE	IDENTIFIER
Experimental models: Cell lines		
3T3-L1 cells	ATCC	Cat#CL-173
$TIRR^{fl/fl}$ MEFs	This paper	N/A
$TIRR^{KO}$ MEFs	This paper	N/A
$p53^{KO}$;$TIRR^{KO}$ MEFs	This paper	N/A
Experimental models: Organisms/strains		
EIIaCre mice	Jax	stock #003724
CD19-Cre mice	Jax	stock #006785
Adp-Cre mice	Jax	stock #028020
Camk2a-Cre mice	Jax	stock #005359
$p53^{KO}$ mice	Jax	stock #002101
$TIRR^{fl/fl}$ mice	This paper	N/A
$TIRR^{KO}$ mice	This paper	N/A
$p53^{HET}$;$TIRR^{KO}$ mice	This paper	N/A
$p53^{KO}$;$TIRR^{KO}$ mice	This paper	N/A
AdipoQ-$Cre^{TG/WT}$;$TIRR^{fl/fl}$ mice	This paper	N/A
Camk2a-$Cre^{TG/WT}$;$TIRR^{fl/fl}$ mice	This paper	N/A
$TIRR^{Bcell\ KO}$ mice	This paper	N/A
Oligonucleotides		
See Table S2 for qPCR and ChIP-qPCR primers	N/A	N/A
Software and algorithms		
Graphpad Prism	Graphpad Software Inc., La Jolla, CA, USA	https://www.graphpad.com
Python, version 3.7.10 pandas, numpy, scipy, statsmodels, sklearn and umap libraries	The Python Software Foundation (PSF)	https://www.python.org
ImajeJ	NIH	https://imagej.nih.gov/ij/